On the role of myosin-induced actin depolymerization during cell migration

Lingxing Yao[a], Yoichiro Mori[b,c], Sean X. Sun[d,e,f], and Yizeng Li[g,*]
[a]Department of Mathematics, University of Akron, Akron, OH 44325; [b]Department of Mathematics and [c]Department of Biology, University of Pennsylvania, Philadelphia, PA 19104; [d]Department of Mechanical Engineering, [e]Institute for NanoBioTechnology, and [f]Center for Cell Dynamics, Johns Hopkins School of Medicine, Baltimore, MD 21205; [g]Department of Biomedical Engineering, Binghamton University, SUNY, Binghamton, NY 13902

ABSTRACT **Mammalian cell migration in open spaces requires F-actin polymerization and myosin contraction. While many studies have focused on myosin's coupling to focal adhesion and stress fibers, the indirect effect of myosin contraction on cell migration through actin depolymerization is not well studied. In this work, we quantified how cell velocity and effective power output are influenced by the rate of actin depolymerization, which is affected by myosin contraction. In addition, we derived scaling laws to provide physical insights into cell migration. Model analysis shows that the cell migration velocity displays a biphasic dependence on the rate of actin depolymerization and myosin contraction. Our model further predicts that the effective cell energy output depends not only on the cell velocity but also on myosin contractility. The work has implications on in vivo processes such as immune response and cancer metastasis, where cells overcome barriers imposed by the physical environment.**

Monitoring Editor
Alex Mogilner
New York University

Received: Nov 1, 2022
Revised: Mar 13, 2023
Accepted: Mar 22, 2023

INTRODUCTION

Mammalian cell migration is important in a number of fundamental in vivo biological processes such as morphogenesis (Mishra *et al.*, 2019a, b), immune response (van der Woude *et al.*, 2017; Baeyens and Schwab, 2020), wound healing (Jorgensen and Sanders, 2016), tissue regeneration (Friedl and Gilmour, 2009), and cancer metastasis (Montell *et al.*, 2012). Actin polymerization and remodeling are central to actin-driven cell migration (Krause and Gautreau, 2014; Inagaki and Katsuno, 2017; Schaks *et al.*, 2019). Multiple factors are known to influence the rate of polymerization and depolymerization, including actin monomer (G-actin) concentration, the presence of major accessory proteins (Alberts *et al.*, 2014), ATP concentration (Atkinson *et al.*, 2004), and importantly, myosin activities (Vallotton *et al.*, 2004; Guha *et al.*, 2005; Medeiros *et al.*, 2006; Haviv *et al.*, 2008; Wilson *et al.*, 2010). Nonmuscle myosin II (hereafter abbreviated as myosin), when activated by myosin light-chain kinase, is a motor protein that generates contractile stress in the actin network (Vicente-Manzanares *et al.*, 2009; Houdusse and Sweeney, 2016).

The impact of myosin on cell migration has been studied from several perspectives. In the canonical cell migration model, myosin retracts the rear end of the cell and moves the cell forward (Mattila and Lappalainen, 2008; Chi *et al.*, 2014; Thomas *et al.*, 2015). In this process, myosin engages with focal adhesions and stress fibers to transfer forces from the extracellular matrix to the cell body (Vicente-Manzanares *et al.*, 2007; Doyle *et al.*, 2012; Bera *et al.*, 2022). The contraction of myosin also elevates the intracellular pressure to push the nucleus (Petrie *et al.*, 2014; Sao *et al.*, 2019) or provides a pulling force for the nucleus (Mistriotis *et al.*, 2019). Besides, myosin contraction acting on the cell membrane can lead to local pressure accumulation and blebbing (Charras *et al.*, 2005), which provides an alternative amoeboid mechanism of cell migration (Bergert *et al.*, 2012; Paluch and Raz, 2013; Muñoz-López *et al.*, 2022).

In addition to directly generating matrix-coupled forces for cell migration, myosin contraction indirectly affects cell migration by promoting the depolymerization of F-actin (Vallotton *et al.*, 2004; Guha *et al.*, 2005; Medeiros *et al.*, 2006; Haviv *et al.*, 2008; Wilson *et al.*, 2010), which affects the rates of actin retrograde flow and treadmilling (Maity *et al.*, 2022). The actin retrograde flow affects the focal adhesion traction force (Gardel *et al.*, 2008), which modulates cell migration velocity (Li and Sun, 2018). Thus the myosin-induced

This article was published online ahead of print in MBoC in Press (http://www.molbiolcell.org/cgi/doi/10.1091/mbc.E22-10-0494) on March 29, 2023.

Data availability: All the equations and parameters that were used to generate the results were represented in the paper. Original codes written in Matlab are available upon request.

*Address correspondence to: Yizeng Li (yli33@binghamton.edu).

Abbreviations used: ATP, adenosine triphosphate; F-actin, filamentous actin; G-actin, monomeric actin.

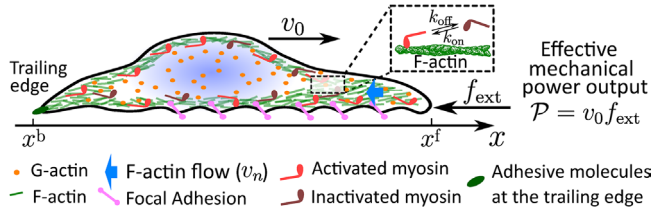

FIGURE 1: Schematics of an actomyosin-driven cell migration model. f_{ext} is the effective external force on the cell from the environment. This force can be used to calculate the effective mechanical power output, $\mathcal{P}$, of a migrating cell at velocity v_0.

actin depolymerization is expected to impact cell velocity. However, due to the indirect relation on cell migration, how myosin contraction-induced actin depolymerization influences cell migration remains unclear.

Moreover, cell migration requires energy to overcome the physical barriers imposed by the environment (Bi *et al.*, 2014; Zhang *et al.*, 2019). The ability to output mechanical energy against the surrounding affects a cell's mobility in complex in vivo environments. For example, during metastasis, cancer cells are capable of navigating through a dense tumor, which has high hydraulic pressure and fluid viscosity (Young *et al.*, 1950; Nathanson and Nelson, 1994; Heldin *et al.*, 2004; Munson and Shieh, 2014; Libutti *et al.*, 2018; Gonzalez-Molina *et al.*, 2018). But the same fluid environment can prevent drugs from being delivered into the tumor. This phenomenon indicates the importance of having active mechanisms that generate mechanical energy in cell migration. However, the role of myosin contractility in cell energy output has not been investigated. In this work, we provide a theoretical framework to elucidate the impact of myosin contraction in modulating actin dynamics and cell migration. We further use our model to analyze the effective force and power output (Recho *et al.*, 2014) generated by a migrating cell with different levels of myosin activity and contractile stress (Figure 1). The physiology- and continuum mechanics-based model demonstrates that the cell velocity is a biphasic function of the rate of actin depolymerization and myosin contraction. The predicted velocity trend is also compared with existing experimental data. Through analysis, we further demonstrate that cell velocity is not the sole indicator of the effective cell mechanical energy output; myosin contractility also influences the potential of a cell to overcome the energy barrier from the extracellular matrix. Our results have implications on how myosin is involved in cell migration in complex in vivo physical environments.

MATHEMATICAL MODELING METHOD

In this *Method* section, we provide a detailed biological description of the model along with the modeling assumptions and implications of such assumptions. The details of the equations and derivations are not included in the main text but can be found in the Supplemental Material. Readers who are more interested in the biological messages inferred from the model, instead of the model development, should feel free to go directly to the *Results* section without reading the entire section on the *Mathematical Modeling Method*. With that being said, reading the first subsection *Model overview* will still help understand the results.

Model overview

Here we describe a multicomponent theoretical model to study how myosin contraction-induced actin depolymerization influences mammalian cell migration. To gain *analytical* insights and obtain useful *scaling* relations, we choose to reduce the computational domain to a one-dimensional space along the *x*-direction. This approach differs from a well-mixed model where the actin and myosin concentrations are taken as constants (Lee *et al.*, 2017). In our model, all the field variables vary along the *x*-direction, which is the direction of cell migration. The model is applicable to studying cell migration where the changes or field variables in the transverse direction are negligible or for cells under narrow confinement in channels or three-dimensional matrices (Petrie *et al.*, 2012, 2014; Stroka *et al.*, 2014; Zhang *et al.*, 2022; Bera *et al.*, 2022). Although this model is primarily developed for a whole cell, the theoretical framework can also be used to model the lamellipodium region of a cell (Krause and Gautreau, 2014) or a cell fragment (Kozlov and Mogilner, 2007; Ofer *et al.*, 2011).

We consider a scenario of directional cell migration where cells and the extracellular environment interaction converges to a steady state (Van Helvert *et al.*, 2018). In this case, the cell velocity, v_0, and the cell length, $x^f(t) - x^b(t) = L$, are constants (Figure 1). We use superscripts "f" and "b" to represent quantities associated with the front and back ends of the cell, respectively. The front and back are defined by the direction of cell migration. This work focuses on actomyosin-driven migration where water permeation across the cell membrane is negligible so that the velocity of the cytosol, v_c, follows the velocity of the cell, i.e., $v_c = v_0$. Under this condition, the cytosol phase can be removed from the model. Models including cytosol, water permeation, solute diffusion, and osmosis can be found in our prior works (Li and Sun, 2018; Li *et al.*, 2019; Bera *et al.*, 2022; Maity *et al.*, 2022; Yao and Li, 2022; Zhang *et al.*, 2022;).

The current model includes the following components that are distributed across the one-dimensional cell along the *x*-direction: F-actin of concentration $\theta_n(x)$, G-actin of concentration $\theta_c(x)$, activated, F-actin attached myosin of concentration $m_n(x)$, and inactivated, free-form myosin of concentration $m_c(x)$. The F-actin concentration refers to the concentration of actin molecules in the filamentous form, not the concentration of actin filaments. The use of the subscript "*n*" refers to the components associated with the actin network, such as the F-actin and activated myosin; whereas "*c*" refers to the components in the cytosolic form, such as the G-actin and inactivated myosin. In the model, we do not distinguish different subtypes of myosin, such as myosin IIA or IIB (Even-Ram *et al.*, 2007). Thus we consider a generic myosin that carries the primary function of providing contractility to the actin network. We do not include microtubules or other structures that can interact with actin and myosin. These elements can be considered in future models.

Forces in the actin network

The F-actin and the activated myosin form a fluidlike actin network. The existence of the actin filament provides a passive swelling stress, σ_n. The passive stress can be modeled by a linear constitutive relation, $\sigma_n = k_{\sigma_n}\theta_n$, where k_{σ_n} is the coefficient of actin swelling. A more involved constitutive relation from polymer physics can be used as well (Li *et al.*, 2019). The activated myosin provides active contractile stress (Vicente-Manzanares *et al.*, 2009; Houdusse and Sweeney, 2016), σ_a, which depends on the concentration of activated myosin. Without loss of generality, we let $k_{\sigma_a} m_n$, where k_{σ_a} is the coefficient of myosin contraction. Alternative expressions of σ_a are possible but will keep our conclusion the same as long as σ_a is an increasing function of m_n. Both k_{σ_n} and k_{σ_a} are positive constants. We can thus express the total stress in the actin network as $\sigma = \sigma_n - \sigma_a$.

While we can see that the stress of the actin network is explicitly affected by k_{σ_n} and k_{σ_a} through the constitutive relations, other factors will implicitly influence the actin network stress through the distribution of θ_n and m_n. These factors include but are not limited to the rates of actin polymerization and depolymerization, myosin activation and inactivation rates, the strength of focal adhesion, etc. For example, in our early work, we have shown that as the rate of actin polymerization increases, F-actin becomes more polarized toward the front, where the concentration of F-actin increases (Yao and Li, 2022). Therefore our model also produces an increased actin network stress at the front as the rate of actin polymerization increases.

The actin network connects to the extracellular matrix via focal adhesions (Stricker *et al.*, 2010). As cells migrate, focal adhesions exert an effective body force on the actin network in the opposite direction of the actin flow, v_n. The magnitude of the body force depends on the magnitude of the actin flow and the distribution of the actin network. It can be modeled by $\eta_{st}\,\theta_n\,v_n$ (Li *et al.*, 2019; Yao and Li, 2022), where η_{st} is the coefficient of focal adhesion, which depends on the substrate stiffness (Bangasser *et al.*, 2017; Walcott and Sun, 2010) and the size (Kim and Wirtz, 2013) and density (Cavalcanti-Adam *et al.*, 2007) of adhesions. In this work, we treat η_{st} as a parameter and do not include the dynamics of focal adhesion (Barnhart *et al.*, 2011).

Although we do not explicitly model the cytosol, we consider the existence of the cytosol as it moves with the cell. The relative velocity between the cytosol velocity, v_c (=v_0), and the actin network produces a frictional force on the actin network, $\eta\theta_n\,(v_n - v_c)$, where η is the coefficient of interfacial friction. This frictional force also serves as an effective body force on the actin network (Dembo and Harlow, 1986). Putting all the forces together, we can write out the force balance of the actin network,

$$-\frac{d\sigma}{dx} - \eta\theta_n(v_n - v_c) - \eta_{st}\theta_n v_n = 0 \qquad (1)$$

This equation will be coupled to the rest of the system to solve for the spatial variables.

F-actin and G-actin exchange and mass balance

Actin polymerization and depolymerization are essential to actomyosin-based cell migration. Polymerization typically occurs at the cell's front edge, whereas depolymerization occurs throughout the cytoplasm. Depolymerization can be considered a sink for F-actin but a source for G-actin. The amount of actin depolymerization per unit of time depends on the concentration of F-actin, which can be represented by $\gamma\theta_n$, where γ is the rate of actin depolymerization. Thus the material balance for F-actin and G-actin is

$$\frac{d}{dx}(\theta_n v_n) = -\gamma\theta_n,$$

$$\frac{d}{dx}(\theta_c v_c) = D_{\theta_c}\frac{d^2}{dx^2}\theta_c + \gamma\theta_n \qquad (2)$$

where D_{θ_c} is the diffusion coefficient of G-actin in the cytosol.

The contribution of actin polymerization is modeled through the flux boundary conditions of Eq. 2. At the front of the cell, the flux boundary condition for F-actin is $\theta_n(v_n - v_0)\big|_{x=x^f} = -J^f_{\text{actin}}$ (Li *et al.*, 2019), where J^f_{actin} is the rate of actin polymerization. We assume that the rate of actin polymerization increases with the concentration of G-actin, θ_c, and saturates when θ_c is large. Therefore J^f_{actin} takes the form $J^f_{\text{actin}} = J_a\theta^f_c/(\theta_{c,c} + \theta^f_c)$, where J_a is the coefficient of actin polymerization and $\theta_{c,c}$ is a constant; θ^f_c is the concentration of G-actin at the front of the cell, i.e., $\theta^f_c = \theta_c\big|_{x=x^f}$. Similarly, the flux boundary condition for G-actin is $\left[-D_{\theta_c}d\theta_c/dx + \theta_c(v_c - v_0)\right]\big|_{x=x^f} = J^f_{\text{actin}}$. Since there is no polymerization at the back of the cell, the fluxes for F-actin and G-actin are zero at $x = x^b$.

Within the timescale of consideration, the total amount of actin is conserved so that the average concentration of actin, θ_*, should be a constant, i.e., $\int_{x^b}^{x^f}(\theta_n + \theta_c)\,dx = L\theta_*$. In the model, θ_* is prescribed but θ_c and θ_n are solved.

The rate of actin depolymerization, γ, depends on multiple factors (Blanchoin *et al.*, 2000). One major factor is the contractile stress in the actin network coming from activated myosin that promotes actin depolymerization (Guha *et al.*, 2005; Medeiros *et al.*, 2006; Yogurtcu *et al.*, 2012; Ganzinger *et al.*, 2019). In a minimal cell migration model where myosin is not considered, the rate of actin depolymerization can be a prescribed number. In a full cell migration model with myosin, we let γ take the form $\gamma = \gamma_0 + \gamma_a\sigma_a$, where γ_0 represents a constant, myosin-independent, baseline rate of actin depolymerization; $\gamma_a\sigma_a$ is a contractility-induced rate of depolymerization; γ_a, the coefficient of contractility-induced depolymerization, is a constant.

Diffusion-convection-reaction of myosin

Activated and inactivated myosin, m_n and m_c, constantly interconvert in the cytoplasm. The kinetic reaction for myosin can be schematically written as $m_c + \theta_n \rightleftharpoons m_n$ (Sakamoto *et al.*, 2011). From this reaction, the activation rate of myosin is $k_{on}\,m_c\theta_n$ and the deactivation rate is $k_{off}\,m_n$, where k_{on} and k_{off} are the rate constant of myosin activation and deactivation, respectively.

The activated myosin attaches to F-actin and is also convected by the F-actin of velocity v_n, whereas the inactivated myosin is convected by the cytosol of velocity v_c. Therefore the steady-state diffusion-convection-reaction equations of the activated and inactivated myosin are

$$\frac{d}{dx}(v_n m_n) = D_{m_n}\frac{d^2 m_n}{dx^2} + k_{on}m_c\theta_n - k_{off}m_n$$
$$\frac{d}{dx}(v_c m_c) = D_{m_c}\frac{d^2 m_c}{dx^2} - k_{on}m_c\theta_n + k_{off}m_n \qquad (3)$$

where D_{m_n} and D_{m_c} are diffusion coefficients. The boundary conditions for Eq. 3 are zero fluxes at both front and back. Total myosin is also conserved so that the average concentration of myosin, m_*, is a constant, i.e., $\int_{x^b}^{x^f}(m_n + m_c)\,dx = Lm_*$.

Force balance of the cell

At the back of the cell, F-actin adheres to the substrate through transmembrane proteins (integrins), which provide an adhesive force, F^b_{ad}, that resists cell migration. We let the adhesive force be proportional to the cell velocity, i.e., $F^b_{ad} = k_{ad}v_0$, where k_{ad} is the coefficient of adhesive force. This adhesive force is physically equivalent to the effective frictional force between the cell and the substrate. Sometimes cells experience external forces at the front during migration, such as forces from other cells, physical obstacles, or experimentally added forces from atomic force microscopy or optical twisters. We use f^f_{ext} to represent such an opposing force per unit area at the front of the cell (Figure 1).

To establish a force balance relation of the cell, we can draw a free-body diagram of the cell and collect all the forces applied to the cell either from the extracellular matrix or through other external means. Any internal forces within the cell should be excluded when analyzing a free-body diagram. This also means the choices of the constitutive relations for the actin network, such as actin swelling and myosin contraction, do not affect the force balance of the cell. In the Supplemental Material, we provide a full discussion on the

Parameters	Description	Values	Sources
L (μm)	Cell length	50	Generic
$\eta\ (\mathrm{Pa\cdot s/\mu m^2/mM})$	Drag coefficient between two phases	1×10^{-2}	Dembo and Harlow (1986)
$\eta_{st}\ (\mathrm{Pa\cdot s/\mu m^2/mM})$	Coefficient of drag from focal adhesion	1×10^{4}	Gardel *et al.* (2008)
k_{σ_n} (Pa/mM)	Coefficient for the passive F-actin stress	1×10^{4}	See text (varied)
$k_{ad}\ (\mathrm{Pa\cdot s/\mu m})$	Coefficient of adhesive force in $F_{ad}^{b}=k_{ad}v_0$	3×10^{4}	See text (varied)
θ_* (mM)	Average concentration of the total actin	0.3	Based on Pollard *et al.* (2000)
$\theta_{c,c}$ (μM)	Critical value of actin polymerization	0.2	Pollard *et al.* (2000)
m_* (mM)	Average concentration of the total myosin	0.01	Based on Barua *et al.* (2014)
J_a (nm mM/s)	Coefficient in $J_{actin}^{f}=J_a\theta_c^{f}/(\theta_{c,c}+\theta_c^{f})$	6	See text
γ_0 (1/s)	Baseline rate of actin depolymerization	1×10^{-4}	See text (varied)
γ_a (1/Pa/s)	Myosin-dependent coefficient of actin depolymerization	2×10^{-3}	See text
k_{on} (1/s/mM)	Coefficient for myosin activation	1	Assumed (varied)
k_{off} (1/s)	Coefficient for myosin deactivation	1.5	Assumed (varied)
D_θ ($\mu m^2/s$)	Diffusion coefficient of G-actin	10	Kiuchi *et al.* (2011)
D_{m_c} ($\mu m^2/s$)	Diffusion coefficient of deactivated myosin	1	See text
D_{m_n} ($\mu m^2/s$)	Diffusion coefficient of activated myosin	0.1	See text

TABLE 1: Model parameters. Unless otherwise specified or varied, these are the default parameters used in the models.

difference between internal and external forces in analyzing a free-body diagram.

In the absence of f_{ext}^{f}, the force balance of the cell is $-\eta_{st}\int_{x^b}^{x^f}\theta_n v_n\,dx=k_{ad}v_0$. The cell velocity, v_0, can be implicitly solved as a function of $\theta_n v_n$ integrated over the space. With the external force, the force balance becomes

$$-\eta_{st}\int_{x^b}^{x^f}\theta_n v_n\,dx=k_{ad}v_0+f_{ext}^{f}. \tag{4}$$

In this case, the external force also directly affects the velocity of cell migration, in addition to the distribution of $\theta_n v_n$, the strength of focal adhesion, η_{st}, and the adhesive coefficient, k_{ad}.

Solving equations

Two types of solutions are presented in this work: numerical and analytical. The numerical results are fully based on the original nonlinear equations and boundary conditions. The one-dimensional cell is discretized into elements where the Finite Difference Method is applied. Our model outputs, or unknowns, are $\theta_n(x)$, $\theta_c(x)$, $m_n(x)$, $m_c(x)$, $v_n(x)$, and v_0. The entire system is solved with the Newton–Raphson iteration scheme. Other variables are expressed in terms of the unknowns or are considered model parameters. All the results (line plots and contour plots) presented in the main text come from numerical solutions.

We also obtain analytical solutions to gain mathematical insights into the scaling laws and the leading-order solutions. All analytical solutions are derived in the Supplemental Material. In the main text, we cite the important results from the analysis but do not go through the details. For a minimal model without myosin, we can obtain closed-form, approximated analytical solutions based on each parameter regime. The analytical solution from the minimal model provides the scaling laws. For a model with myosin, we obtain the leading-order solution based on the asymptotic analysis.

Model parameters

All the parameters used in the model are listed in Table 1. Unless otherwise specified or varied, these are the default values representing a typical mammalian cell. Parameters denoted as "varied" will serve as independent variables, and the cell velocity or other dependent quantities will be plotted as functions of these independent variables. Below are a few comments on the choice of parameters.

The estimation of the coefficient of actin polymerization, J_a, comes from the actin flux boundary condition at the leading edge, i.e., $\theta_n^{f}(v_n^{f}-v_0)=-J_{actin}^{f}$, where $J_{actin}^{f}=J_a\theta_c^{f}/(\theta_{c,c}+\theta_c^{f})$. Since $\theta_{c,c}\ll\theta_c^{f}$ (Pollard *et al.*, 2000), then $J_{actin}^{f}\approx J_a$. The quantity $(v_n^{f}-v_0)$ at the cell's leading edge is the actin retrograde flow, which can vary from about 20 nm/s up to the order of 100 nm/s (Kiuchi *et al.*, 2007; Chan and Odde, 2008; Gardel *et al.*, 2008; Vitriol *et al.*, 2015; Bangasser *et al.*, 2017). The concentration of F-actin at the cell's leading edge also varies and is typically on the order of a few μM (Koestler *et al.*, 2009). The value of J_a can thus be estimated by the product of the actin retrograde flow velocity and the concentration of F-actin. The value of J_a used in this work is meant to produce actin retrograde flow up to about 100 nm/s; the exact value depends on the rate of actin depolymerization. We can increase J_a if a higher rate of actin retrograde flow is desired. In this case, the velocity of cell migration will also increases accordingly.

The ratio of k_{σ_n} and η_{st} has a dimension of length^2/time, which is the dimension of the diffusion coefficient. Indeed, k_{σ_n}/η_{st} serves as the effective diffusion coefficient for the F-actin (see the Supplemental Material analysis). The numerical stability of the model

requires that this effective diffusion coefficient cannot be too small. After careful numerical testings and estimation of passive actin network stress, we found 10^4 Pa/mM to be a propitiate order of magnitude for the coefficient of passive F-actin stress, k_{σ_n}. Since the concentration of F-actin is on the order of 0.01–0.1 mM (Satcher and Dewey, 1996; Pollard *et al.*, 2000), this value of k_{σ_n} corresponds to a passive actin network swell pressure of 0.1–1 kPa. Although there is no direct measurement of the passive actin pressure, experiments that poke the actin network to measure its elasticity also fall in the range up to 1 kPa (Gardel *et al.*, 2006; Chaudhuri *et al.*, 2007). Hence we believe that the k_{σ_n} value we are using is within the reasonable range. We can also use a higher value of k_{σ_n} than what is currently being used without negatively impacting the numerical stability of the model. In this case, the corresponding passive pressure of F-actin will increase but will not change the conclusions and predictions from our model.

The adhesive force provides resistance to cell migration. So the coefficient of adhesive force, k_{ad}, modulates the overall velocity of cell migration. We choose $k_{\text{ad}} = 3 \times 10^4$ Pa·s/μm so that the predicted cell velocity is on the order of 20–30 nm/s, which is the typical velocity of a generic mammalian epithelial cell. When necessary, we can increase the predicted cell velocity by either decreasing k_{ad} or increasing the coefficient of actin polymerization, J_a, without changing the rest of the system. But the choice of k_{ad} or J_a is not central to this work.

The estimation of the diffusion coefficient of deactivated myosin, D_{m_c}, and activated myosin, D_{m_n}, is based on the diffusion coefficient of G-actin, D_{θ_c}. We let $D_{m_n} \ll D_{m_c}$ and $D_{m_c} \ll D_{\theta_c}$ to reflect the physical nature of the molecules.

The rate of actin depolymerization, γ, in the minimal model and the coefficient of myosin contraction, k_{σ_a}, in the full model are the two most essential parameters in the study. We let these two parameters vary across several orders of magnitudes. These values can be found in the *Results* section below. In the full model, two additional parameters, γ_0 and γ_a, also affect the total rate of actin depolymerization. However, since we vary the myosin contraction, k_{σ_a}, over several orders of magnitudes, k_{σ_a} plays a central role in determining the total rate of actin depolymerization. In this regard, the two parameters, γ_0 and γ_a, are nominal, and their values are assumed.

This work focuses on qualitative trends of cell response as a function of several parameters. The trends can be nonlinear, monotonic, biphasic, polarized, or anything cells adapt as a process changes. We found that the trends predicted by our model are robust and independent of our parameter choice as long as the model remains numerically stable.

RESULTS

We start with a minimal model where only actin is present and myosin is not coupled to the system (without Eq. 3 and $\sigma = \sigma_n$). We also neglect the external force, $f^{\text{f}}_{\text{ext}}$ (Figure 1), for the moment. This system provides a theoretical basis for understanding the impact of actin depolymerization on cell velocity. We then analyze the fully coupled model with myosin contraction and discuss the physiological relevance and significance. At the end, we consider the cell mechanical energy output by adding an external force.

Actin depolymerization polarizes F-actin

In the minimal model, the rate of actin depolymerization, γ, is independent of myosin. We examine the case where γ is spatially constant. The model predicts that the concentration of F-actin, θ_n, decreases with increasing γ (Figure 2a). When γ is small, the overall concentration of F-actiin is high. It is slightly polarized at the two ends of the cell, forming an almost symmetric spatial distribution with respect to the center of the cell (see the Supplemental Material for an analytical solution). As γ increases, F-actin moves toward a small region at the cell front and becomes highly polarized. In this case, the spatial distribution of F-actin decays exponentially from the leading edge to the interior. The predicted exponential decay is consistent with experimental observations from keratocyte fragments, where the actin intensity was found to decay exponentially front the leading edge to the back (Ofer *et al.*, 2011). Since the passive actin swell stress, σ_n, increases with the concentration of F-actin, the spatial distribution of F-actin also shows the polarized distribution of σ_n.

The actin network flows from the cell's leading edge toward the interior, known as actin retrograde flow (Gardel *et al.*, 2008). The velocity of this F-actin retrograde flow, v_n, is predicted to decrease from the leading edge toward the back of the cell (Figure 2b). This prediction is also consistent with experimental observations from keratocyte fragments (Ofer *et al.*, 2011). In addition, the model found that the magnitude of the actin retrograde flow increases with γ (Figure 2b). This is because, for the same amount of actin flux at the cell front, low F-actin concentration leads to a high actin flow because of the flux boundary conditions.

The biphasic cell velocity

With these predicted features of F-actin distribution and flow, we perform the following analysis on cell velocity.

Small γ limit. When the rate of actin depolymerization approaches zero ($\gamma \to 0$), which can happen when F-actin is immobilized, the concentration of G-actin approaches zero ($\theta_c \to 0$). This means that almost all the actin is in filamentous form. Since the total amount of actin is conserved at the timescale of consideration, the concentration of F-actin thus approaches the total actin concentration ($\theta_n \to \theta_*$). This can also be inferred from Figure 2a where θ_n becomes less polarized and approaches to $\theta_* = 300$ μM (Table 1) as $\gamma \to 0$. In particular, as shown by the analysis, when $\gamma << J_a/(\theta_* L)$, we have $\theta^{\text{f}}_c \ll \theta_{c,c}$. This is a low G-actin regime in which $J^{\text{f}}_{\text{actin}}$ increases linearly with θ_c. In this case, the F-actin velocity, or the retrograde flow, is found to be a linear function in space, $v_n \approx -\gamma x + v_0$, on the scale of γL. This linear analytical approximation of F-actin velocity is consistent with our numerical calculation (Figure 2b).

Under these approximations, the cell velocity, v_0, is solved as

$$v_0 = \frac{\eta_{\text{st}}\theta_* L}{k_{\text{ad}} + \eta_{\text{st}}\theta_* L}\left(\frac{\gamma L}{2}\right), (v_0 \propto \gamma) \tag{5}$$

which is an increasing function of the rate of actin depolymerization, γ. Since θ_* is essentially θ_n under small γ limit, the product $\theta_* L$ represents the content of F-actin. The term $\eta_{\text{st}}\theta_* L$ indicates the capacity of cell migration under the influence of forces from focal adhesions (η_{st} is the coefficient of focal adhesion). The cell velocity increases with the combined effort of focal adhesion strength and the content of F-actin.

Large γ limit. When $\gamma >> J_a/(\theta_* L)$, we have $\theta^{\text{f}}_c >> \theta_{c,c}$. This is a high G-actin regime in which $J^{\text{f}}_{\text{actin}}$is approximately a constant. Analysis shows that there is a length scale $\ell = \sqrt{k_{\sigma_n}/((\eta + \eta_{st})\gamma)}$ that shrinks as γ, the rate of actin depolymerization, increases. This is the "effective" cell length or the length of F-actin distribution. For example, at a low rate of actin depolymerization, the distribution of F-actin is not polarized, and F-actin occupies the entire cell (Figure 2a). In this case, the effective cell length is the same as the physical cell length. At a high rate of actin depolymerization, F-actin

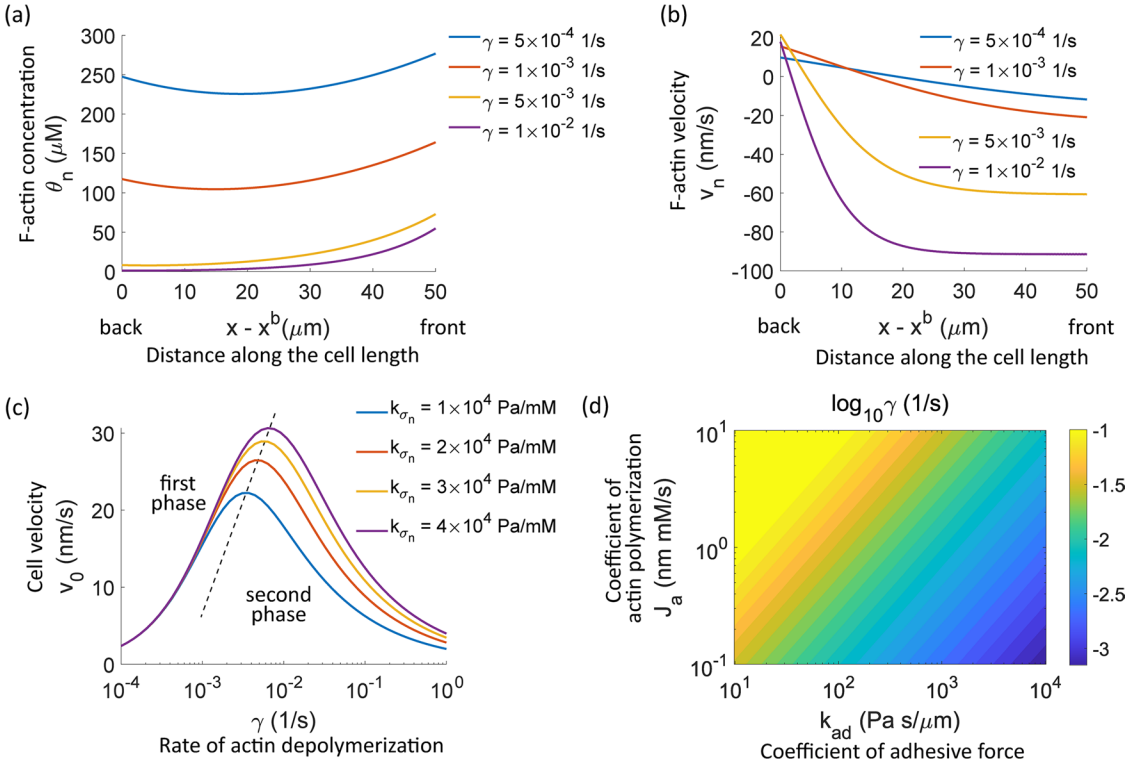

FIGURE 2: Prediction from a minimal model with actin only. (a) Spatial distribution of F-actin concentration θ_n. (b) Spatial distribution of F-actin velocity v_n in a fixed frame. In a moving frame with the cell, the F-actin velocity is shifted by $v_n - v_0$ i.e., at the back of the cell, the relative actin velocity to the cell is 0. In (a) and (b), $x = 0$ and $x = 50$ μm represent the back and front of the cell, respectively. (c) Cell velocity is biphasic in the rate of actin depolymerization, γ. (d) The contour of $\log_{10}\gamma$ gives the maximum cell velocity in the biphasic response as a function of the coefficient of actin polymerization and the coefficient of adhesive force.

polarizes to the front of the cell and only occupies the front region of the cell. In this case, the effective cell length reduces to a fraction of the cell at the front. Since the reactive force from focal adhesions is transmitted through the F-actin, the effective cell length indicates the spatial span of the cell that is able to carry forces to contribute to actomyosin-driven cell migration.

When $\ell/L \ll 1$, meaning the physical cell length is much larger than the effective cell length, we find an approximate solution of cell velocity as

$$v_0 = \frac{\eta_{st} J^f_{actin}}{k_{ad}}\ell, \ \left(v_0 \propto \gamma^{-1/2}\right) \tag{6}$$

which is a decreasing function of the rate of actin depolymerization, γ. This expression also suggests that the strength of focal adhesion, η_{st}, and the rate of actin polymerization, J^f_{actin}, serve as driving forces of cell migration.

Biphasic cell velocity on γ. The above analysis shows that the cell velocity is biphasic in the rate of actin depolymerization, γ: at the small-γ limit, the cell velocity increases with γ linearly, whereas at the large-γ limit, the cell velocity decreases with γ in an inverse square root manner. This analysis result can be seen from the numerical calculation of cell velocity as a function of γ (Figure 2c). The physical interpretation of this biphasic behavior is as follows.

For cells to experience sufficient force from focal adhesions, the cell must maintain a sufficient actin retrograde flow (Li and Sun, 2018). When γ is small (the rising phase in Figure 2c), most of the actin is in the filamentous form, which provides abundant connections to focal adhesions (Thievessen *et al.*, 2013). In addition, the effective cell length is the entire physical length of the cell. In this case, the effective cell length is not the limiting factor, but the actin retrograde flow starts to influence cell speed. We see in the analysis that the actin retrograde flow scales with γ*L* for a low rate of actin depolymerization, which leads to a linear relationship between cell velocity and γ*L* (Eq. 5), or γ. When γ is large (the declining phase in Figure 2c), most of the actin is in the monomeric form, which leads to polarized F-actin distribution toward the cell front. In this case, the effective length of the cell, scaled by $\gamma^{-1/2}$, becomes the dominant factor for cell velocity (Eq. 6).

The model suggests that the interplay of F-actin redistribution and the rate of the actin retrograde flow produces a transition from retrograde flow-dominated regimes to effective cell length-dominated regimes of cell migration. In the retrograde flow-dominated regime, increasing the rate of actin depolymerization helps develop the flow, leading to the first phase of cell migration. In the cell length-dominated regime, increasing the rate of actin depolymerization reduces cell length, leading to the second phase of cell migration.

Biphasic cell protrusion velocity has also been predicted in models where the number of barbed ends was considered (Mogilner and Edelstein-Keshet, 2002). Cells need a sufficient number of barbed ends to provide protrusive force, but too many barbed ends lead to G-actin depletion and cell velocity reduction. Models based on G-actin availability (Mogilner and Edelstein-Keshet, 2002) and our model are developed from different prospectives and approaches but are related when considering actin dynamics and structure. For

example, for a large number of barbed ends, where G-actin is depleted, the actin retrograde flow is predicted to be small, corresponding to the low cell velocity predicted in our model. On the other hand, for a low number of barbed ends, where actin protrusive force is insufficient, the connection between the actin network and focal adhesion is projected to be limited, which also corresponds to short cell length and low velocity in our model.

Actin network relaxation increases cell velocity

The analysis shows that the effective cell length, ℓ, increases with the coefficient of passive actin stress, k_{σ_n}. This is because the passive actin stress enhances mechanical relaxation within the actin network.

At low rates of actin depolymerization, where the F-actin spreads across the cell, the effective cell length is the same as the physical cell length. In this case, we do not expect k_{σ_n} to have an impact on cell velocity (Eq. 5). At high rates of actin depolymerization, where the effective cell length increases with k_{σ_n}, we also expect the same trend for cell velocity (Eq. 6). Numerical calculation confirmed the analysis (Figure 2c). We see that the coefficient of passive actin stress does not influence the cell velocity for low rates of actin depolymerization but starts to play a role as the rate increases. In particular, the impact of k_{σ_n} is most significant around the maximum cell velocity and diminishes as the rate of actin depolymerization continues to increase. The diminishment is due to the reduced F-actin content at a high rate of actin depolymerization.

The γ value that gives the maximum cell velocity depends on multiple factors. We have already seen that k_{σ_n} moves the peak to the large end of γ (Figure 2c). Increasing the coefficient of actin polymerization, J_a, or decreasing the coefficient of adhesive force, k_{ad}, also moves the peak to the large end of γ (Figure 2d). Models based on G-actin availability also predicted that the peak of biphasic cell velocity depends on the membrane resistance (Mogilner and Edelstein-Keshet, 2002).

Myosin contractility does not affect force balance at the cellular level

We next consider a model where myosin is included (with Eq. 3 and $\sigma = \sigma_n - \sigma_a$). We first examine a hypothetical case of a constant rate of actin depolymerization, γ, i.e., we implement the myosin component in the model but dissociate the rate of actin depolymerization with myosin. This step aims to clarify whether myosin contraction *directly* affects cell migration through its mechanical effect.

It might be tempting to expect that myosin contractility is part of the force balance and thus influences cell migration. The numerical calculation indicates that when the rate of actin depolymerization is low, the cell velocity is almost independent of myosin contractility, k_{σ_a} (Figure 3a). Asymptotic analysis on small perturbation of the rate of actin polymerization and depolymerization also shows that the leading-order solution for the cell velocity is independent of k_{σ_a}. As the rate of actin depolymerization increases to an intermediate range, the myosin contractility starts to reduce cell velocity slightly, but this only happens at the large end of k_{σ_a} (Figure 3a). This slight reduction of cell velocity comes from a slightly reduced effective cell length due to the opposite effect of actin relaxation, i.e., the effect of antirelaxation. Further increasing the actin depolymerization rate reduces myosin contractility's contribution to cell velocity (Figure 3a).

The result shown in Figure 3a may appear unexpected. As discussed above, the distribution of F-actin and the actin retrograde flow affect cell migration. When the rate of actin depolymerization is dissociated with myosin contractility, the distribution of F-actin and the actin retrograde flow are barely affected by myosin contractility for the most part. In the Supplemental Material, we have more discussion on why the internal stress of the actin network does not directly affect the cell force balance. Only when the stress is significant enough to modulate the cell effective cell length will the cell velocity be able to change. For example, we have seen that actin passive swelling helps to relax the actin network and increase the effective cell length, increasing the cell velocity in a γ-dependent manner (Figure 2c). Given the above results, we thus expect that myosin plays a role through other means. Below we will explore the role of myosin contraction through its modulation of the rate of actin depolymerization.

Myosin contraction affects actomyosin distribution and flow

Now we consider a full model with a myosin-dependent rate of actin depolymerization: $\gamma = \gamma_0 + \gamma_a \sigma_a$. γ_0 and γ_a are constants but the myosin contraction, $\sigma_a = k_{\sigma_a} m_n$, is a variable because the activated myosin concentration, $m_n(x)$, depends on multiple factors. We will vary the coefficient of myosin contraction, k_{σ_a}, to modulate the rate of actin depolymerization, γ: large k_{σ_a} leaders to high γ. With the change of myosin contractility, k_{σ_a}, the spatial distribution of F-actin (Figure 3b) follows the same trend as seen in the minimal model (Figure 2a). This model prediction, where myosin contraction breaks down the actin network, also matches experimental observations on an actin cortex model where the intensity of the actin network decreases with increasing contraction from myosin (Ganzinger *et al.*, 2019). Observations on keratocytes also showed that myosin disassembles the actin network (Wilson *et al.*, 2010). Since in our model myosin is activated on F-actin, the activated myosin distribution follows the F-actin trend (Figure 3c). The active stress, $\sigma_a = k_{\sigma_a} m_n$, still increases with the contractility k_{σ_a} even if the myosin concentration reduces with k_{σ_a}.

Similar to the minimal model, with an increasing myosin-induced actin depolymerization rate, the amplitude of actin retrograde flow increases (Figure 3d). The analysis also indicates that myosin contractility has a leading-order effect on the actin retrograde flow through the rate of actin depolymerization. From modeling perspectives, the actin retrograde flow can be incorporated from either a kinematic or kinetic perspective. We model the actin flow from an actin flux kinematic boundary condition. Models based on kinetic relation and myosin contraction have also been developed (Barnhart *et al.*, 2011). An alternative approach is to develop a kinematic relation for the actin flow through the kinetics of myosin contraction (Chan and Odde, 2008; Bangasser *et al.*, 2017). Although different approaches have been used to model the actin retrograde flow, the conclusions remain consistent that high myosin contraction increases actin retrograde flow, while suppressing myosin activity reduces the flow (Cai *et al.*, 2006; Yang *et al.*, 2012).

Myosin contraction leads to biphasic cell velocity via actin depolymerization

Analysis indicates that the leading-order solution for the cell velocity is affected by both γ_0 and the myosin contractility, k_{σ_a}. The latter increases the total rate of actin depolymerization, γ. Numerical solutions of the model predict that the cell velocity, v_0, is biphasic in k_{σ_a} (Figure 3e) in a similar manner as the biphasic response in γ in the minimal model (Figure 2c). We discuss the implications of this result in the *Discussion* section. Models showing a bifurcation distribution of myosin (Kruse and Jülicher, 2003; Recho *et al.*, 2013, 2015) can provide an alternative mechanism for the biphasic cell velocity in myosin contractility.

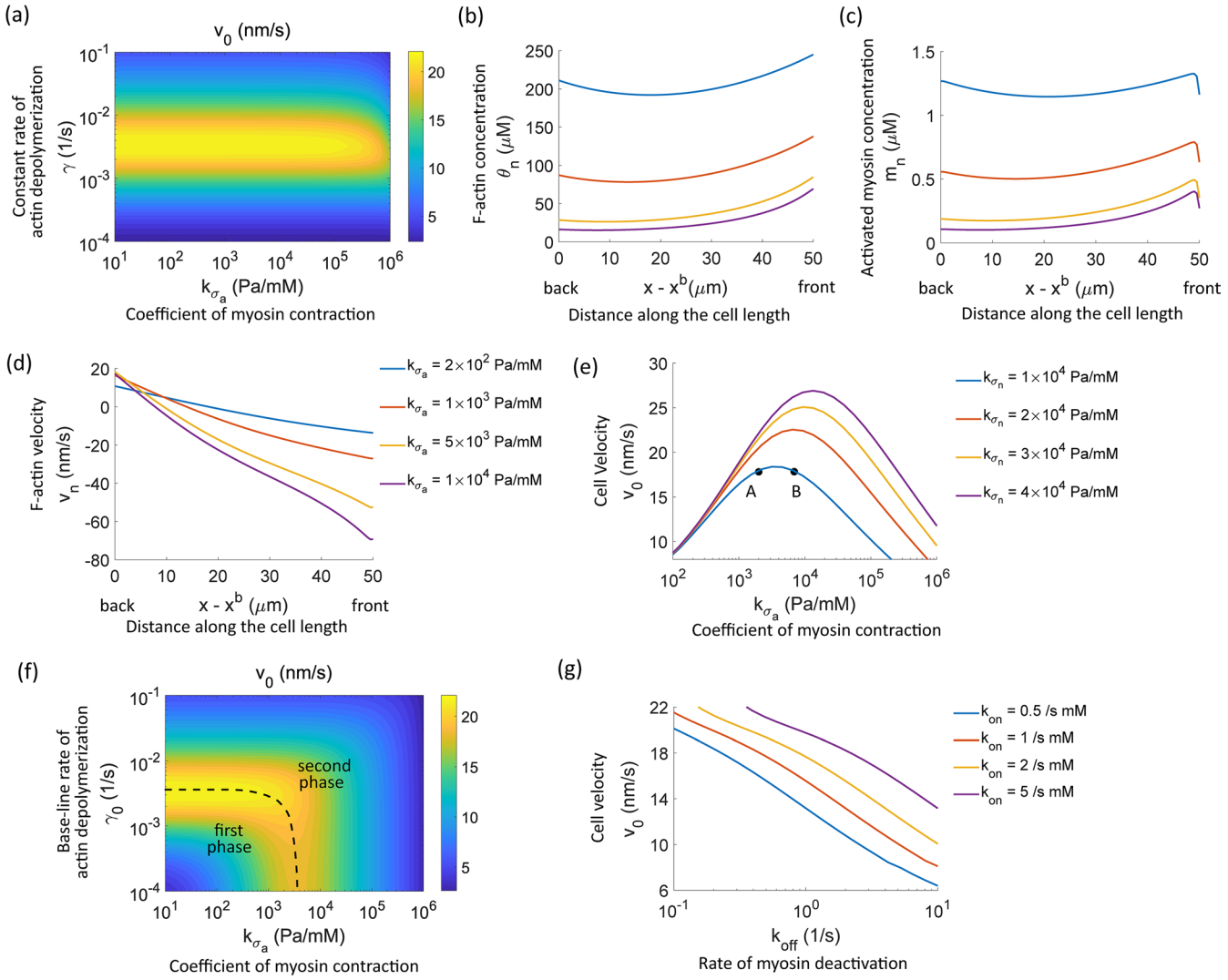

FIGURE 3: Predictions from a full model with myosin. (a) Cell velocity as a function of a constant rate of actin depolymerization, γ, and the coefficient of myosin contraction, k_{σ_a}. (b)–(d) Spatial distribution of the concentration of F-actin (b), the concentration of activated myosin (c), and the velocity of F-actin (d) for different values of the coefficient of myosin contraction, k_{σ_a}; $x = 0$ and $x = 50$ μm represent the back and front of the cell, respectively. The legend of color lines in (d) applies to all three panels (b)–(d); $\gamma_0 = 5 \times 10^{-4}$ 1/s. (e) Cell velocity is biphasic in the coefficient of myosin contraction, k_{σ_a}. The two points, A and B, correspond to the curves A and B in Figure 4(c), respectively. (f) Cell velocity contour as a function of the baseline rate of actin depolymerization (γ_0) and the coefficient of myosin contraction (k_{σ_a}) shows dual biphasic curves. (g) Cell velocity as a function of the rate of myosin deactivation, k_{off}, for different rates of myosin activation, k_{on}; $k_{\sigma_a} = 500$ Pa/mM is within the first-phase regime in (f).

The influence of the coefficient of passive actin swelling stress, k_{σ_n}, on the full model is the same as that in the minimal model (Figures 3e and 2c). Both γ_0 and k_{σ_a} have the potential to impact cell velocity in a biphasic manner (Figure 3f). However, the biphasic response does not always occur. For example, when k_{σ_a} is large, the cell velocity is monotonic in γ_0 (Figure 3f). Likewise, when γ_0 is large, the cell velocity is monotonic in k_{σ_a}. For extremely large γ_0 such that $\gamma_0 >> \gamma_a \sigma_a$, γ is dominated by γ_0 so the effect of k_{σ_a} on cell velocity is negligible. In this case, myosin contraction is not predicted to affect cell velocity. Myosin-independent cell migration has been observed in mice bone marrow-derived dendrite cells. Inhibiting myosin II by blebbistatin did not affect cell velocity when the cells were not physically confined (Barbier *et al.*, 2019). Although it was not clear why myosin was not involved in this particular case, it could be that when mature dendrite cells spread on open two-dimensional spaces, myosin II did not directly participate in the rate of actin depolymerization and retrograde flow.

The rates of myosin activation, k_{on}, and deactivation, k_{off}, are present in the leading-order solution for the cell velocity when the system is perturbed on the rate of actin polymerization and depolarization. Within the first phase in Figure 3f, increasing the rate of myosin deactivation leads to a decrease in cell velocity through decreased myosin concentration and thus the rate of actin depolymerization. For the same reason, increasing the rate of myosin activation leads to an increase in cell velocity (Figure 3g). Since myosin dynamics are controlled by multiple intracellular variables such as pH, calcium concentration, and ATP (Doyle *et al.*, 2012), the model suggests a mechanism with which cells can modulate their speed.

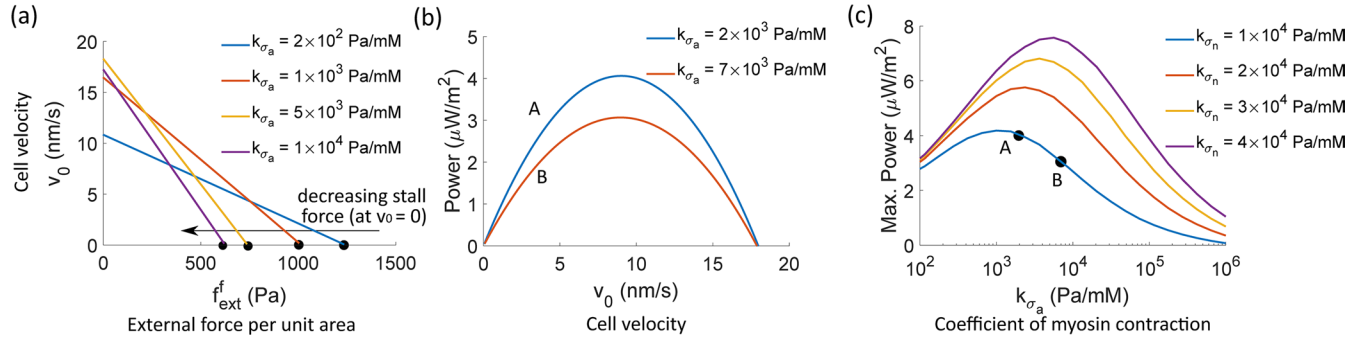

FIGURE 4: (a) Cell velocity as a function of the external force for different coefficients of myosin contraction k_{σ_a}. (b) The mechanical power output of cell migration as a function of cell velocity. Line A is in the first phase, and line B is in the second phase but has the same baseline velocity as line A in the first phase (see points A and B in Figure 3e). (c) Maximal power output as a function of the coefficient of myosin contraction k_{σ_a}. Points A and B correspond to the same myosin contractility as the points in Figure 3e.

Stall force decreases monotonically with myosin contractility

Stall force, f^f_{stall}, is defined as the force stalls cell migration. It estimates the ability of the cell to overcome physical barriers in the extracellular environment. In our model, we apply an opposing external force per unit area at the front of the cell, f^f_{ext} (Figure 1). When the external force is absent, meaning $f^f_{ext} = 0$, we define the cell velocity as the baseline velocity. The velocities predicted in Figures 2 and 3 are all baseline velocities. As the external force increases from zero, the cell velocity will decrease and eventually come to a stop. We can plot the cell velocity as a function of the external force and obtain the stall force per unit area when the cell stalls, i.e., $v_0 = 0$.

The model predicts that the stall force decreases monotonically with increasing myosin contractility (Figure 4a), although in the first phase, the cell baseline velocity increases with k_{σ_a} (Figure 3e). This result indicates that the stall force does not necessarily correlate with the cell velocity. In other words, the cell velocity alone does not reflect the ability of the cell to overcome external physical barriers.

An analytical solution from the minimal model shows the same trend of the stall force in the rate of actin depolymerization, γ,

$$f^f_{stall} = \eta_{st} J^f_{actin} \ell \tanh\left(\frac{L}{2\ell}\right), \qquad \ell = \sqrt{\frac{k_{\sigma_n}}{(\eta + \eta_{st})\gamma}} \tag{7}$$

which decreases monotonically for all $\gamma > 0$ even though the cell velocity is biphasic in γ. The result suggests that with the increasing rate of actin depolymerization, less force is needed to stall cell migration, implying that cells with decreasing F-actin concentration have a reduced ability to overcome physical barriers in the environment.

The expression of the stall force per unit area, or stall pressure, from the minimal model (Eq. 7) indicates that the magnitude of the pressure depends on multiple factors, including the strength of focal adhesion, the rate of actin polymerization, and the effective cell length. The stall pressure calculated from the model is on the order of 1 kPa, consistent with the stall pressure measured from keratocytes (Prass *et al.*, 2006). Different cell types may exhibit different interactions with the substrate or distinct patterns of F-actin distribution, which can alter the magnitude of the stall pressure. For example, the stall pressure estimated from fibroblasts is on the order of 10 kPa (Abraham *et al.*, 1999), one magnitude higher than the stall pressure measured from keratocytes (Prass *et al.*, 2006). Interestingly, keratocytes are known as the fastest migrating cells, yet the stall pressure measured from keratocytes is one order of magnitude lower than that of fibroblasts. This nonintuitive result supports our model prediction that cell velocity alone does not reflect the ability of the cell to overcome external physical barriers (Figure 4a).

Mechanical power output is biphasic in myosin contractility

Cell migration consumes energy (Lodish *et al.*, 2004; Zanotelli *et al.*, 2018; Zhang *et al.*, 2019) and outputs mechanical work (Li *et al.*, 2019). The power output can be quantified similarly to a car engine, where the engine rotational speed is measured against the applied resistance. In this work, we will calculate the effective cell output power by multiplying the external force and the corresponding cell velocity, i.e., Power = $f^f_{ext} v_0$. To obtain a relation between the power output and the cell velocity, we vary the external force from 0 up to the stall force. By doing so, the cell velocity changes from the baseline velocity to 0 (Figure 4a). We know that when $f^f_{ext} = 0$ or $v_0 = 0$, the product is 0.

The model shows that the effective cell output power is quadratic in v_0 (Figure 4b). For the same baseline velocity on the two sides of the biphasic velocity curve, the mechanical power output in the second phase (Figure 4b line B, corresponding to the point B in Figure 3e) is uniformly reduced compared with that in the first phase (Figure 4b line A, corresponding to the point A in Figure 3e). This is a direct result of the reduced ability of the cell to overcome physical barriers as myosin contractility increases (Figure 4a).

Each of the quadratic curves of power output has a maximum value. The model predicts that the maximum power output is also biphasic in myosin contractility, k_{σ_a}, and increases with the coefficient of passive actin stress, k_{σ_n}. The location of the peaks in the maximum power shifts toward the smaller values of k_{σ_a} (Figure 4c) than that in the maximum velocity (Figure 3e). This shift comes from the reduced ability of cells to overcome external forces with increasing k_{σ_a}.

DISCUSSION

Scaling laws and the underlying physics

We derived several scaling relations that provide physical insights into the mechanics behind actomyosin-driven cell migration. The mechanisms behind the two-phase cell velocity are the effects of the actin retrograde flow and the distribution of F-actin. In the small-γ limit, the average actin retrograde velocity is $\overline{\gamma}_n \approx -\gamma L/2 + v_0$. We can substitute $\overline{\gamma}_n$ into Eq. 5 and rewrite the cell velocity as $v_0 = (\eta_{st}/k_{ad})(\theta_* |\overline{v}_n|) L$. From this expression, we can see that when F-actin is distributed throughout the cell, i.e., the effective cell length is the original cell length ($\ell = L$), the cell velocity is proportional to the magnitude of the actin retrograde flow. At the large-γ limit, as shown in Eq. 6, the cell velocity is proportional to the effective cell length, ℓ. Together, we can express the cell velocity as

$$v_0 = \begin{cases} (\eta_{st}/k_{ad})(\theta_* |\overline{v}_n|) L & \text{small } \gamma \text{ limit} \\ (\eta_{st}/k_{ad})(J^f_{actin}) \ell & \text{large } \gamma \text{ limit} \end{cases} \tag{8}$$

In a more descriptive way, based on Eq. 8, the cell velocity is scaled by

$$v_0 \propto \frac{(\text{focal adhesion})(\text{actin flow})}{\text{resistance}}(\text{effective cell length}) \quad (9)$$

The product of the "focal adhesion" and "actin flow" provides the "driving force" of actomyosin-driven cell migration, whereas the "effective cell length" magnifies or shrinks the driving force. The biphasic cell velocity predicted by the model is thus a result of the interplay between the actin flow and the effective cell length, i.e., $|\bar{v}_n|$ increases with γ, whereas ℓ decreases with γ.

The stall force is predicted to decrease monotonically with the rate of actin depolymerization. In Eq. 7, the "tanh" term is dimensionless and saturates as the argument increases. We thus neglect this factor in our discussion and only focus on the first three factors. Our $J^{\mathrm{f}}_{\mathrm{actin}}$ is the material flux with a dimension of (concentration)·(velocity). ℓ is an effective cell length, and we assume that the cross-sectional area of the cell is constant. So the product of $J^{\mathrm{f}}_{\mathrm{actin}}\ell$ is proportional to the total material of F-actin times a velocity. Since the total material represents the total mass, the product $J^{\mathrm{f}}_{\mathrm{actin}}\ell$ is also proportional to the effective momentum of F-actin. Together, we can scale the stall force by

$$f^{\mathrm{f}}_{\mathrm{stall}} \propto (\text{focal adhesion})(\text{F}-\text{actin momentum}) \quad (10)$$

This scaling relation suggests that cells' ability to overcome physical barriers in the environment depends on the strength of focal adhesion and the momentum of the actin network.

Implications of the scaling laws on cell migration

Myosin plays a vital role in actomyosin-driven cell migration. Experimental observations suggest that how myosin contributes to cell migration depends on the cell type and cell geometry. For example, inhibiting nonmuscle myosin IIA in nonconfined migration of RW4 mouse embryonic stem cells (RW4 ES) (Even-Ram *et al.*, 2007) and NIH 3T3 fibroblasts (Doyle *et al.*, 2012) was found to increase cell velocity. But inhibition of myosin II decreased velocities of nonconfined migration of keratocytes (Wilson *et al.*, 2010). It did not show an effect on the migration of mice bone marrow-derived dendrite cells (mDCs) (Barbier *et al.*, 2019). However, when NIH 3T3 (Doyle *et al.*, 2012) and mDCs (Barbier *et al.*, 2019) migrated in confined spaces, inhibiting myosin IIA decreased cell velocity. These experimental results indicate that myosin contractility can have biphasic effects on cell velocity.

Our model has the potential to provide possible physical explanations behind these observations. For example, as mDCs get more confined, myosin inhibition was more likely to reduce cell velocities compared with nonconfined cells (Barbier *et al.*, 2019). We know that cells under confinement are polarized (Stroka *et al.*, 2014; Mistriotis *et al.*, 2019; Zhao *et al.*, 2019, 2022; Bera *et al.*, 2022). The directionality of the actin retrograde flow, which is along the cell length, is prominent under confined geometry. In this case, inhibiting myosin is expected to reduce the actin flow along the cell, leading to a reduced cell velocity based on Eq. 9. This may also be the case for NIH 3T3 cells under confinement (Doyle *et al.*, 2012).

Cell migration on nonconfined space exhibits different morphology. RW4 ES cells with knocked-out myosin IIA displayed elongated and protrusive cell shape and increased cell velocity (Even-Ram *et al.*, 2007). The relation between cell elongation and increased velocity can potentially be explained by Eq. 9. Keratocytes, on the other hand, displayed shortened front-to-rear cell length upon myosin II inhibition (Wilson *et al.*, 2010). Interestingly, keratocytes were found to have decreased cell velocity upon myosin inhibition. In a separate study on keratocytes fragments, the speed of the fragments was also found to increase with the front-to-rear length of the fragments (Ofer *et al.*, 2011). All these results suggest that the cell velocity was correlated with the effective cell length along the direction of cell migration, as predicted by Eq. 9.

Model limitations and future development

In our model, the myosin plays two roles: providing contractile stress for the actin network and promoting actin depolymerization through myosin contraction. We do not explicitly connect myosin to the substrate, only implicitly through the distribution of F-actin. As a result, myosin contractile stress is an internal stress within the cell and is *indirectly* linked to the extracellular environment. So the major contribution from myosin is influencing the rate of actin depolymerization. We have assumed a steady-state cell migration so that the cell length remains constant. If the cell length could extend or shrink depending on myosin contractility, myosin may have additional effects on cell migration. Moreover, we have left out components such as water flux, osmosis (Li *et al.*, 2020), myosin-dependent adhesion dynamics (Vicente-Manzanares *et al.*, 2007; Doyle *et al.*, 2012; Craig *et al.*, 2015; Murrell *et al.*, 2015; Swaminathan *et al.*, 2017), membrane-tension-dependent actin polymerization (Tsujita *et al.*, 2015), and substrate physical properties (Chan and Odde, 2008; Bangasser *et al.*, 2017). These components can be incorporated into future studies.

CONCLUSION

In this work, we developed a multiphase cell migration model, which includes F-actin, G-actin, activated myosin, and nonactivated myosin, to study the relationship between cell velocity and actin depolymerization. Although this model is primarily developed for a whole cell, the theoretical framework is also applicable to modeling the lamellipodium region of a cell (Krause and Gautreau, 2014) or a cell fragment (Kozlov and Mogilner, 2007; Ofer *et al.*, 2011). The model predicts that myosin contraction can increase the rate of actin depolymerization and modulate cell velocity in a biphasic manner, which is rooted in the interplay of actin flow and the redistribution of F-actin. However, cell velocity alone does not determine the effective mechanical power output of cell migration. For example, even if cells migrate at the same velocity (on the two sides of the biphasic velocity curve), the effective cell energy outputs are distinct, as high myosin contractility leads to low migratory energy output at the same velocity. This result has implications on how cells in vivo such as neutrophils during immune response (van der Woude *et al.*, 2017; Baeyens and Schwab, 2020) or cancer cells during metastasis (Montell *et al.*, 2012) design their intracellular machinery to achieve a desired migratory outcome. For instance, to migrate at the same velocity, cells might stay in the first phase to obtain sufficient mechanical power output to navigate challenging physical environments. Since myosin contractility reduces F-actin concentration by increasing the actin depolymerization rate, the model suggests that the F-actin content indicates cells' ability to overcome external barriers. This is consistent with the physical explanation from the minimal model that the strength of the connection between focal adhesion and F-actin affects cell velocity. Therefore the model suggests that the F-actin content indicates cells' ability to overcome external barriers. Understanding the roles of myosin contraction in cell migration will also help design physics-based, bio-inspired robots for advanced health therapy.

ACKNOWLEDGMENTS

Lingxing Yao is supported by NSF-DMS 1852597. Sean X. Sun is supported by NIH R01GM134542. Yizeng Li is supported by NSF 2303648. The opinions, findings, and conclusions, or recommendations expressed are those of the authors and do not necessarily reflect the views of any of the funding agencies.

REFERENCES

Abraham VC, Krishnamurthi V, Taylor DL, Lanni F (1999). The actin-based nanomachine at the leading edge of migrating cells. Biophys J 77, 1721–1732.

Alberts B, Johnson A, Lewis J, Morgan D, Raff M, Roberts K, Walter P (2014). Molecular Biology of the Cell, Garland Science, New York.

Atkinson SJ, Hosford MA, Molitoris BA (2004). Mechanism of actin polymerization in cellular ATP depletion. J Biol Chem 279, 5194–5199.

Baeyens AAL, Schwab SR (2020). Finding a way out: S1P signaling and immune cell migration. Annu Rev Immunol 38, 759–784.

Bangasser BL, Shamsan GA, Chan CE, Opoku KN, Tüzel E, Schlichtmann BW, Kasim JA, Fuller BJ, McCullough BR, Rosenfeld SS, Odde DJ (2017). Shifting the optimal stiffness for cell migration. Nat Commun 8, 15313.

Barbier L, Sa´ez PJ, Attia R, Lennon-Dume´nil A-M, Lavi I, Piel M, Vargas P (2019). Myosin II activity is selectively needed for migration in highly confined microenvironments in mature dendritic cells. Front Immunol 10, 747.

Barnhart EL, Lee K-C, Keren K, Mogilner A, Theriot JA (2011). An adhesion-dependent switch between mechanisms that determine motile cell shape. PLoS Biol 9, e1001059.

Barua B, Nagy A, Sellers JR, Hitchcock-DeGregori SE (2014). Regulation of nonmuscle myosin ii by tropomyosin. Biochemistry 53, 4015–4024.

Bera K, Kiepas A, Godet I, Li Y, Mehta P, Ifemembi B, Paul CD, Sen A, Serra SA, Stoletov K, *et al*. (2022). Extracellular fluid viscosity enhances cell migration and cancer dissemination. Nature 611, 365–373.

Bergert M, Chandradoss SD, Desai RA, Paluch E (2012). Cell mechanics control rapid transi-tions between blebs and lamellipodia during migration. Proc Natl Acad Sci USA 109, 14434–14439.

Bi D, Lopez JH, Schwarz JM, Manning ML (2014). Energy barriers and cell migration in densely packed tissues. Soft matter 10, 1885–1890.

Blanchoin L, Pollard TD, Mullins RD (2000). Interactions of ADF/cofilin, Arp2/3 complex, capping protein and profilin in remodeling of branched actin filament networks. Curr Biol 10, 1273–1282.

Cai Y, Biais N, Giannone G, Tanase M, Jiang G, Hofman JM, Wiggins CH, Silberzan P, Buguin A, Ladoux B, Sheetz MP (2006). Nonmuscle myosin IIA-dependent force inhibits cell spreading and drives F-actin flow. Biophys J 91, 3907–3920.

Cavalcanti-Adam EA, Volberg T, Micoulet A, Kessler H, Geiger B, Spatz JP (2007). Cell spreading and focal adhesion dynamics are regulated by spacing of integrin ligands. Biophys J 92, 2964–2974.

Chan CE, Odde DJ (2008). Traction dynamics of filopodia on compliant substrates. Science 322, 1687–1691.

Charras GT, Yarrow JC, Horton MA, Mahadevan L, Mitchison TJ (2005). Non-equilibration of hydrostatic pressure in blebbing cells. Nature 435, 365–369.

Chaudhuri O, Parekh SH, Fletcher DA (2007). Reversible stress softening of actin networks. Nature 445, 295–298.

Chi Q, Yin T, Gregersen H, Deng X, Fan Y, Zhao J, Liao D, Wang G (2014). Rear acto-myosin contractility-driven directional cell migration in three-dimensional matrices: a mechano-chemical coupling mechanism. J R Soc Interface 11, 20131072.

Craig EM, Stricker J, Gardel M, Mogilner A (2015). Model for adhesion clutch explains biphasic relationship between actin flow and traction at the cell leading edge. Phys Biol 12, 035002.

Dembo M, Harlow F (1986). Cell motion, contractile networks, and the physics of interpenetrating reactive flow. Biophys J 50, 109–121.

Doyle AD, Kutys ML, Conti MA, Matsumoto K, Adelstein RS, Yamada KM (2012). Micro-environmental control of cell migration–myosin IIA is required for efficient migration in fibrillar environments through control of cell adhesion dynamics. J Cell Sci 125, 2244–2256.

Even-Ram S, Doyle AD, Conti MA, Matsumoto K, Adelstein RS, Yamada KM (2007). Myosin IIA regulates cell motility and actomyosin–microtubule crosstalk. Nat Cell Biol 9, 299–309.

Friedl P, Gilmour D (2009). Collective cell migration in morphogenesis, regeneration and cancer. Nat Rev Mol Cell Biol 10, 445.

Ganzinger KA, Vogel SK, Mücksch J, Blumhardt P, Schwille P (2019). Myosin-II activity generates a dynamic steady state with continuous actin turnover in a minimal actin cortex. J Cell Sci 132.

Gardel ML, Nakamura F, Hartwig J, Crocker JC, Stossel TP, Weitz DA (2006). Stress-dependent elasticity of composite actin networks as a model for cell behavior. Phys Rev Lett 96, 088102.

Gardel ML, Sabass B, Ji L, Danuser G, Schwarz US, Waterman CM (2008). Traction stress in focal adhesions correlates biphasically with actin retrograde flow speed. J Cell Biol 183, 999–1005.

Gonzalez-Molina J, Zhang X, Borghesan M, da Silva JM, Awan M, Fuller B, Gavara N, Selden C (2018). Extracellular fluid viscosity enhances liver cancer cell mechanosensing and migration. Biomaterials 177, 113–124.

Guha M, Zhou M, Wang Y-L (2005). Cortical actin turnover during cytokinesis requires myosin II. Curr Biol 15, 732–736.

Haviv L, Gillo D, Backouche F, Bernheim-Groswasser A (2008). A cytoskeletal demolition worker: myosin II acts as an actin depolymerization agent. J Mol Biol 375, 325–330.

Heldin C-H, Rubin K, Pietras K, Östman A (2004). High interstitial fluid pressure—an obstacle in cancer therapy. Nat Rev Cancer 4, 806–813.

Houdusse A, Sweeney HL (2016). How myosin generates force on actin filaments. Trends Biochem Sci 41, 989–997.

Inagaki N, Katsuno H (2017). Actin waves: Origin of cell polarization and migration? Trends Cell Biol 27, 515–526.

Jorgensen SN, Sanders JR (2016). Mathematical models of wound healing and closure: a comprehensive review. Med Biol Eng Comput 54, 1297–1316.

Kim D-H, Wirtz D (2013). Focal adhesion size uniquely predicts cell migration. FASEB J 27, 1351–1361.

Kiuchi T, Nagai T, Ohashi K, Mizuno K (2011). Measurements of spatiotemporal changes in g-actin concentration reveal its effect on stimulus-induced actin assembly and lamellipodium extension. J Cell Biol 193, 365–380.

Kiuchi T, Ohashi K, Kurita S, Mizuno K (2007). Cofilin promotes stimulus-induced lamellipodium formation by generating an abundant supply of actin monomers. J Cell Biol 177, 465–476.

Koestler SA, Rottner K, Lai F, Block J, Vinzenz M, Small JV (2009). F-and G-actin concentrations in lamellipodia of moving cells. PloS one 4, e4810.

Kozlov MM, Mogilner A (2007). Model of polarization and bistability of cell fragments. Biophys J 93, 3811–3819.

Krause M, Gautreau A (2014). Steering cell migration: lamellipodium dynamics and the regulation of directional persistence. Nat Rev Mol Cell Biol 15, 577–590.

Kruse K, Jülicher F (2003). Self-organization and mechanical properties of active filament bundles. Phys Rev E 67, 051913.

Lee W, Lim S, Kim Y (2017). The role of myosin II in glioma invasion: A mathematical model. PLoS One 12, e0171312.

Li Y, Konstantopoulos K, Zhao R, Mori Y, Sun SX (2020). The importance of water and hydraulic pressure in cell dynamics. J Cell Sci 133, jcs240341.

Li Y, Sun SX (2018). Transition from actin-driven to water-driven cell migration depends on external hydraulic resistance. Biophys J 114, 2965–2973.

Li Y, Yao L, Mori Y, Sun SX (2019). On the energy efficiency of cell migration in diverse physical environments. Proc Natl Acad Sci USA 116, 23894–23900.

Libutti SK, Tamarkin L, Nilubol N (2018). Targeting the invincible barrier for drug delivery in solid cancers: interstitial fluid pressure. Oncotarget 9, 35723.

Lodish H, Berk A, Matsudaira P, Kaiser CA, Krieger M, Scott MP, Zipursky L, Darnell J (2004). Molecular Cell Biology, San Francisco: Freeman.

Maity D, Bera K, Li Y, Ge Z, Ni Q, Konstantopoulos K, Sun SX (2022). Extracellular hydraulic resistance enhances cell migration. Adv Sci 9, 2200927.

Mattila PK, Lappalainen P (2008). Filopodia: molecular architecture and cellular functions. Nat Rev Mol Cell Biol 9, 446–454.

Medeiros NA, Burnette DT, Forscher P (2006). Myosin II functions in actin-bundle turnover in neuronal growth cones. Nat Cell Biol 8, 216–226.

Mishra AK, Campanale JP, Mondo JA, Montell DJ (2019a). Cell interactions in collective cell migration. Development 146.

Mishra AK, Mondo JA, Campanale JP, Montell DJ (2019b). Coordination of protrusion dynamics within and between collectively migrating border cells by myosin II. Mol Biol Cell 30, 2490–2502.

Mistriotis P, Wisniewski EO, Bera K, Keys J, Li Y, Tuntithavornwat S, Law RA, Perez-Gonzalez NA, Erdogmus E, Zhang Y, *et al*. (2019). Confinement hinders motility by inducing rhoa-mediated nuclear influx, volume expansion, and blebbing. J Cell Biol 218, 4093–4111.

Mogilner A, Edelstein-Keshet L (2002). Regulation of actin dynamics in rapidly moving cells: a quantitative analysis. Biophys J 83, 1237–1258.
Montell DJ, Yoon WH, Starz-Gaiano M (2012). Group choreography: mechanisms orchestrating the collective movement of border cells. Nat Rev Mol Cell Biol 13, 631–645.
Muñoz-López MJ, Kim H, Mori Y (2022). A reduced 1d stochastic model of bleb-driven cell migration. Biophys J 121, 1881–1896.
Munson JM, Shieh AC (2014). Interstitial fluid flow in cancer: implications for disease progression and treatment. Cancer Manag Res 6, 317.
Murrell M, Oakes PW, Lenz M, Gardel ML (2015). Forcing cells into shape: the mechanics of actomyosin contractility. Nat Rev Mol Cell Biol 16, 486–498.
Nathanson SD, Nelson L (1994). Interstitial fluid pressure in breast cancer, benign breast conditions, and breast parenchyma. Ann Surg Oncol 1, 333–338.
Ofer N, Mogilner A, Keren K (2011). Actin disassembly clock determines shape and speed of lamellipodial fragments. Proc Natl Acad Sci 108, 20394–20399.
Paluch EK, Raz E (2013). The role and regulation of blebs in cell migration. Curr Opin Cell Biol 25, 582–590.
Petrie RJ, Gavara N, Chadwick RS, Yamada KM (2012). Nonpolarized signaling reveals two distinct modes of 3D cell migration. J Cell Biol 197, 439–455.
Petrie RJ, Koo H, Yamada KM (2014). Generation of compartmentalized pressure by a nuclear piston governs cell motility in a 3D matrix. Science 345, 1062–1065.
Pollard TD, Blanchoin L, Mullins RD (2000). Molecular mechanisms controlling actin filament dynamics in nonmuscle cells. Annu Rev Biophys Biomol Struct 29, 545–576.
Prass M, Jacobson K, Mogilner A, Radmacher M (2006). Direct measurement of the lamellipodial protrusive force in a migrating cell. J Cell Biol 174, 767–772.
Recho P, Joanny J-F, Truskinovsky L (2014). Optimality of contraction-driven crawling. Phys Rev Lett 112, 218101.
Recho P, Putelat T, Truskinovsky L (2013). Contraction-driven cell motility. Phys Rev Lett 111, 108102.
Recho P, Putelat T, Truskinovsky L (2015). Mechanics of motility initiation and motility arrest in crawling cells. J Mech Phys Solids 84, 469–505.
Sakamoto Y, Prudhomme S, Zaman MH (2011). Viscoelastic gel-strip model for the simulation of migrating cells. Ann Biomed Eng 39, 2735–2749.
Sao K, Jones TM, Doyle AD, Maity D, Schevzov G, Chen Y, Gunning PW, Petrie RJ (2019). Myosin II governs intracellular pressure and traction by distinct tropomyosin-dependent mechanisms. Mol Biol Cell 30, 1170–1181.
Satcher RL, Dewey CF (1996). Theoretical estimates of mechanical properties of the endothelial cell cytoskeleton. Biophys J 71, 109–118.
Schaks M, Giannone G, Rottner K (2019). Actin dynamics in cell migration. Essays Biochem 63, 483–495.
Stricker J, Falzone T, Gardel ML (2010). Mechanics of the f-actin cytoskeleton. J Biomech 43, 9–14.
Stroka KM, Jiang H, Chen S-H, Tong Z, Wirtz D, Sun SX, Konstantopoulos K (2014). Water permeation drives tumor cell migration in confined microenvironments. Cell 157, 611–623.
Swaminathan V, Kalappurakkal JM, Mehta SB, Nordenfelt P, Moore TI, Koga N, Baker DA, Oldenbourg R, Tani T, Mayor S, *et al.* (2017). Actin retrograde flow actively aligns and orients ligand-engaged integrins in focal adhesions. Proc Natl Acad Sci USA 114, 10648–10653.
Thievessen I, Thompson PM, Berlemont S, Plevock KM, Plotnikov SV, Zemljic-Harpf A, Ross RS, Davidson MW, Danuser G, Campbell SL, Waterman CM (2013). Vinculin-actin interaction couples actin retrograde flow to focal adhesions, but is dispensable for focal adhesion growth. J Cell Biol 202, 163–177.
Thomas DG, Yenepalli A, Denais CM, Rape A, Beach JR, Wang Y-L, Schiemann WP, Baskaran H, Lammerding J, Egelhoff TT (2015). Nonmuscle myosin IIB is critical for nuclear translocation during 3D invasion. J Cell Biol 210, 583–594.
Tsujita K, Takenawa T, Itoh T (2015). Feedback regulation between plasma membrane tension and membrane-bending proteins organizes cell polarity during leading edge formation. Nat Cell Biol 17, 749–758.
Vallotton P, Gupton SL, Waterman-Storer CM, Danuser G (2004). Simultaneous mapping of filamentous actin flow and turnover in migrating cells by quantitative fluorescent speckle microscopy. Proc Natl Acad Sci USA 101, 9660–9665.
van der Woude LL, Gorris MAJ, Halilovic A, Figdor CG, de Vries IJM (2017). Migrating into the tumor: a roadmap for T cells. Trends Cancer 3, 797–808.
Van Helvert S, Storm C, Friedl P (2018). Mechanoreciprocity in cell migration. Nat Cell Biol 20, 8–20.
Vicente-Manzanares M, Ma X, Adelstein RS, Horwitz AR (2009). Non-muscle myosin II takes centre stage in cell adhesion and migration. Nat Rev Mol Cell Biol 10, 778.
Vicente-Manzanares M, Zareno J, Whitmore L, Choi CK, Horwitz AF (2007). Regulation of protrusion, adhesion dynamics, and polarity by myosins iia and iib in migrating cells. J Cell Biol 176, 573–580.
Vitriol EA, McMillen LM, Kapustina M, Gomez SM, Vavylonis D, Zheng JQ (2015). Two functionally distinct sources of actin monomers supply the leading edge of lamellipodia. Cell Rep 11, 433–445.
Walcott S, Sun SX (2010). A mechanical model of actin stress fiber formation and substrate elasticity sensing in adherent cells. Proc Natl Acad Sci 107, 7757–7762.
Wilson CA, Tsuchida MA, Allen GM, Barnhart EL, Applegate KT, Yam PT, Ji L, Keren K, Danuser G, Theriot JA (2010). Myosin II contributes to cell-scale actin network treadmilling through network disassembly. Nature 465, 373.
Yang Q, Zhang X-F, Pollard TD, Forscher P (2012). Arp2/3 complex–dependent actin networks constrain myosin II function in driving retrograde actin flow. J Cell Biol 197, 939–956.
Yao L, Li Y (2022). Effective force generation during mammalian cell migration under different molecular and physical mechanisms. Front Cell Dev Biol 10, 903234.
Yogurtcu ON, Kim JS, Sun SX (2012). A mechanochemical model of actin filaments. Biophys J 103, 719–727.
Young JS, Llumsden CE, Stalker AL (1950). The significance of the "tissue pressure" of normal testicular and of neoplastic (brown-pearce carcinoma) tissue in the rabbit. J Pathol Bacteriol 62, 313–333.
Zanotelli MR, Goldblatt ZE, Miller JP, Bordeleau F, Li J, VanderBurgh JA, Lampi MC, King MR, Reinhart-King CA (2018). Regulation of ATP utilization during metastatic cell migration by collagen architecture. Mol Biol Cell 29, 1–9.
Zhang J, Goliwas KF, Wang W, Taufalele PV, Bordeleau F, Reinhart-King CA (2019). Energetic regulation of coordinated leader–follower dynamics during collective invasion of breast cancer cells. Proc Natl Acad Sci USA 116, 7867–7872.
Zhang Y, Li Y, Thompson KN, Stoletov K, Yuan Q, Bera K, Lee SJ, Zhao R, Kiepas A, Wang Y, *et al.* (2022). Polarized NHE1 and SWELL1 regulate migration direction, efficiency and metastasis. Nat Commun 13, 6128.
Zhao R, Afthinos A, Zhu T, Mistriotis P, Li Y, Serra SA, Zhang Y, Yankaskas CL, He S, Valverde MA, *et al.* (2019). Cell sensing and decision-making in confinement: The role of TRPM7 in a tug of war between hydraulic pressure and cross-sectional area. Sci Adv 5, eaaw7243.